metals

Article

Enhanced Mechanical Properties and Electrical Conductivity in Ultrafine-Grained Al 6101 Alloy Processed via ECAP-Conform

Maxim Murashkin [1,*], Andrey Medvedev [1], Vil Kazykhanov [1], Alexander Krokhin [2], Georgy Raab [1], Nariman Enikeev [3] and Ruslan Z. Valiev [1]

[1] Institute for Physics of Advanced Materials, Ufa State Aviation Technical University, Ufa 450000, Russia; E-Mails: deckard@list.ru (A.M.); vk@mail.rb.ru (V.K.); giraab@mail.ru (G.R.); rzvaliev@mail.rb.ru (R.Z.V.)

[2] United Company RUSAL, Moscow 109240, Russia; E-Mail: aleksandr.krokhin@rusal.com

[3] Laboratory for Mechanics of Bulk Nanostructured Materials, Saint Petersburg State University, Saint-Petersburg 199034, Russia; E-Mail: carabus@mail.rb.ru

* Author to whom correspondence should be addressed; E-Mail: m.murashkin.70@gmail.com; Tel.: +7-3472-734449; Fax: +7-3472-733422.

Abstract: This paper studies the effect of equal channel angular pressing-Conform (ECAP-C) and further artificial aging (AA) on microstructure, mechanical, and electrical properties of Al 6101 alloy. As is shown, ECAP-C at 130 °C with six cycles resulted in the formation of an ultrafine-grained (UFG) structure with a grain size of 400–600 nm containing nanoscale spherical metastable β′ and stable β second-phase precipitates. As a result, processed wire rods demonstrated the ultimate tensile strength (UTS) of 308 MPa and electrical conductivity of 53.1% IACS. Electrical conductivity can be increased without any notable degradation in mechanical strength of the UFG alloy by further AA at 170 °C and considerably enhanced by additional decomposition of solid solution accompanied by the formation of rod-shaped metastable β′ precipitates mainly in the ultrafine grain interior and by the decrease of the alloying element content in the Al matrix. It is demonstrated that ECAP-C can be used to process Al-Mg-Si wire rods with the specified UFG microstructure. The mechanical strength and electrical conductivity in this case are shown to be much higher than those in the industrial semi-finished products made of similar material processed by the conventional T6 or T81 treatment.

1. Introduction

Mechanical strength and electrical conductivity are the most important properties of conducting materials. Al-Mg-Si alloys, such as 6101, 6201, *etc.*, demonstrate an enhanced combination of these properties, and are currently widely used to produce electrical and power conductors of self-supporting insulated lines and overhead power transmission lines [1–5]. The materials are also considered for application as electrical wiring in the car industry [6].

Due to high corrosion resistance, specific strength, and good machinability, as well as lower cost as compared to copper and copper-based alloy conductors, the Al-Mg-Si alloys have become increasingly popular. Thus, the effort to enhance the performance properties of the materials is of particular interest to the scientific and engineering communities in terms of the use of such materials for advanced applications.

As is known, the current-conducting elements made of commercial Al-Mg-Si alloys in the form of a wire of various diameters have yield strength of 275–330 MPa and electrical conductivity of 57.5%–52.0% IACS (International Annealed Copper Standard), correspondingly [2,5]. These properties are achieved through conventional thermo-mechanical processing T81, including quenching, cold drawing, and artificial aging in a sequential order [2,7,8]. The processed microstructure has mainly non-recrystallized grains elongated in the direction of drawing. These grains contain an increased dislocation density and Mg_2Si nanoscale metastable β″ and/or β′ second-phase strengthening precipitates formed along three equivalent directions <001> in the Al matrix of several nm in diameter and up to 100 nm in length [9–14]. The specified level of the material strength can be achieved through dislocation strengthening and precipitation hardening, with enhanced electrical conductivity attained via the decrease in the content of solute Mg and Si atoms in the Al matrix.

As a rule, metallurgical techniques [8,15–17] or modifications of conventional thermo-mechanical processing, for example T6 or T81 [7,18], are currently used to improve the properties of commercial Al-Mg-Si alloys. In [8], it is recommended to modify the cast Al 6201 alloy with boron microadditives to enhance electrical conductivity by decreasing the content of such impurities as Ti, Cr, V, and Mn in an Al solid solution. In [15], the possibility to increase the operating temperature of Al-Mg-Si conductors via additional alloying with Zr and the formation of Al_3Zr dispersed particles is demonstrated. In [16,17], it was shown that the increase in Si excess content could enhance the effect of precipitation hardening due to the formation of nanoscale Si precipitates along with basic strengthening Mg_2Si phases during artificial ageing. However, these techniques cannot enhance both electrical conductivity and strength of conductor materials simultaneously.

Recently, we have proposed a new approach to enhance the properties of commercial Al alloys of the Al-Mg-Si system allowing us to increase both strength and electrical conductivity of the materials. It can be achieved through combination of the UFG structure formation and solid solution decomposition accompanied by the formation of strengthening Mg_2Si phase precipitates of both

metastable and stable modifications using severe plastic deformation (SPD) [19–23]. The strengthening up to 365 MPa can be achieved via grain refinement during SPD, as well as through precipitation hardening induced by following dynamic aging. The research [19–24] has also proved that in parallel with the formation of UFG structure, SPD also considerably accelerates the decomposition of a supersaturated solid solution and contributes to a greater reduction of the content of alloying element atoms in the Al matrix of Al-Mg-Si alloys as compared to conventional processing techniques. In good agreement with the Matthiessen's rule for dilute alloys [25], this leads to the increase in electrical conductivity of UFG alloys up to more than 58% IACS [19–21]. The approach was used to process Al-Mg-Si alloys via such SPD processing techniques as high pressure torsion (HPT) and equal channel angular pressing with parallel channels (ECAP-PC). Due to certain limitations (small size of samples processed, low material utilization ratio, *etc.*) these techniques of processing are regarded as laboratory ones and cannot be applied to commercially produce UFG materials. Apart from that, the ECAP-C technique is capable of producing long-length UFG billets that could be used as ingots for industrial processes [26]. As an example, the given SPD technique allowed producing UFG structures in long-length Ti and Al alloy rods [27–30], as well as in steel ones [31], resulting in a considerable enhancement of both mechanical and service characteristics as compared to similar semi-finished billets processed via conventional techniques.

The main objective of this work is to demonstrate the potential of continuous ECAP-C technique for fabrication of high strength UFG Al 6101 alloy showing a better combination of mechanical strength and electrical conductivity compared to the commercial Al-Mg-Si alloy processed via conventional thermo-mechanical treatments, which are currently used in the electrical engineering.

2. Experimental Section

Commercial Al 6101 alloy in T1 state was used as a material for study (cooled from an elevated temperature shaping process and naturally aged) with a typical chemical content, namely: 0.58 Mg; 0.54 Si; 0.23 Fe; 0.003 Cu; 0.01 Zn; 0.012 (ΣTi + V + Cr + Mn); res. Al (wt. %). The initial material had a form of continuous cast re-draw rolled rods with a diameter of 12.5 mm. The material for investigation was supplied by UC RUSAL (Moscow, Russia).

Initial rods of 1.5 m in length were successively annealed at 550 °C, water quenched and subjected to SPD. To form the UFG structure, quenched billets were SPD-processed by ECAP-C technique. A schematic drawing of the ECAP-C machine is shown in Figure 1a. Initially, a wire rod of 12.5 mm in diameter (1) heated to the specified temperature was placed into a pressing channel comprised of a running wheel die (2), pressure arrangement working surfaces (3), and a gauge (4). Friction resistance forces a wire rod going from a running wheel die (2) into a channel formed by a pressure arrangement (3) and a gauge (4), coupling at a certain angle (ψ) with a wheel die. Shear straining occurs at an intersection of these channels (deformation zone).

ECAP-C machine was used to process wire rods under isothermal conditions at 130 °C. Intersection angle of channels (ψ) (Figure 1a) constituted 120° with six processing cycles corresponding to an equivalent strain of about 4 [32]. A wire rod was rotated around the axis by +90° after each ECAP-C cycle (route *Bc*). According to the previous studies [33,34], it is the most efficient mode to form a homogeneous UFG structure in Al alloys. ECAP-C treatment resulted in the production of rods up to

1.5 m in length with a square cross section of 11 × 11 mm (Figure 1b). No noticeable macro-defects resulting from a deformation processing were observed on the surface (Figure 1b). Some part of the processed wire rods was artificially aged (AA) at the temperatures of 170 ℃ for 1–6 h and at 190 ℃ for 1–12 h.
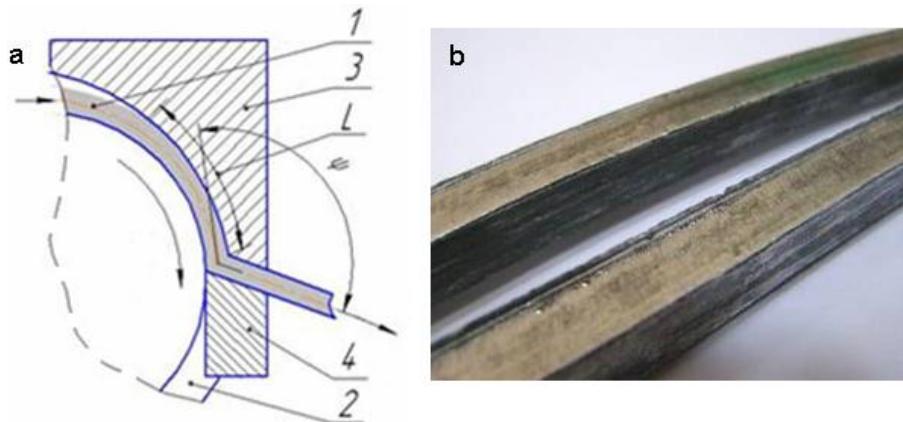
Figure 1. (**a**) A schematic illustration of ECAP-C machine: 1—ingot; 2—running wheel die; 3—pressure arrangement working surface; 4—a gauge; ψ—angle of intersection with a wheel die; *L*—arc of a rod grip; and (**b**) the surface of wire rods of Al 6101 alloy after six cycles of ECAP-C at 130 ℃.

The microstructure of wire rods was studied by transmission and scanning electron microscopy (TEM and SEM). A longitudinal section of wire rods in both the initial state and processed by ECAP-C and AA was analyzed.

TEM investigations were implemented using JEM-2100 electron microscope (JEOL, Tokyo, Japan) at an accelerating voltage of 200 kV. To study the microstructure, thin foils were used, produced by jet polishing on a Tenupol-5 machine (Struers, Ballerupcity, Denmark) with the chemical solution consisting of 20% nitric acid and 80% methanol at a temperature of −25 ℃ and a voltage of 15 V. A mean size of structural elements was determined based on the measurements of at least 200 mean diameters. At least three foils of each state were studied to obtain statistically significant results.

The microstructure homogeneity as well as the distribution of particles of crystallized secondary phases were estimated by SEM using JSM-6490LV (JEOL, Tokyo, Japan) at an accelerating voltage of 20 kV. The chemical composition of secondary phases was analyzed by EDX technique using an extension to INCA electron microscope X-Act by the Oxford Instruments Company, Oxford, UK.

A longitudinal section of the rod in the initial state, as well as processed by SPD and further AA was analyzed.

X-ray studies were performed using Ultima IV diffractometer (Rigaku, Tokyo, Japan) by CuKα irradiation (30 kV and 20 mA). The size of coherent domains (*D*), values of mean-square microdistortion of crystalline lattice ($<\varepsilon^2>^{1/2}$) and crystalline lattice parameter (*a*) were calculated using Rietveld analysis with the help of MAUD software (copyright by L. Lutterotti, Trento, Italy) [35]. To estimate dislocation density (ρ), the Equation (1) was used [36].

$$\rho = 2\sqrt{3}\langle\varepsilon^2\rangle^{1/2} / \left(D \times b\right) \tag{1}$$

where $b = a\sqrt{2}/2$ is the Burgers vector for fcc-metals, D is the coherent domain size.

Mechanical testing was performed at room temperature using Instron 5982 tensile testing machine (Instron Engineering Corporation, Buckinghamshire, UK) with a strain rate of 10^{-3} s^{-1}. Strength (yield strength (YS) and ultimate tensile strength (UTS)) and ductility characteristics (elongation to failure (El.)) of rods were estimated based on tensile testing of the samples with a cylindrical gauge section having 3 mm in diameter and a length of 15 mm and wire samples—with a working part length of 250 mm. To obtain consistent results, at least three samples were tested per each data point.

Electrical resistivity of the material under study was measured in accordance with IEC 60468:1974 standard (CEN, Bruxelles, Belgium) [37]. Straightened samples of at least 1 m long in a measured part were taken.

3. Results and Discussion

3.1. Microstructural Features of the Alloy Processed via ECAP-C

TEM studies revealed an inhomogeneous microstructure with average grain size of 10 μm for Al 6101 alloy in the T1 state processed via a conventional technique (continuous casting and redraw rolling). Grains are elongated along the rolling direction (Figure 2a,b). The metal structure also contains intermetallic crystalline inclusions varying from 0.5 to 5 μm in size oriented along the rolling direction (marked by an arrow) (Figure 2a). This distribution of intermetallic particles is typical for Al semi-finished products processed via pressing or rolling [38]. EDX analysis of particles showed the presence of Fe, Si, and Al with a stoichiometric ratio of 2:2:9. This composition is typical for Al alloys of the Al-Mg-Si system containing no Mn and/or Cr [39].
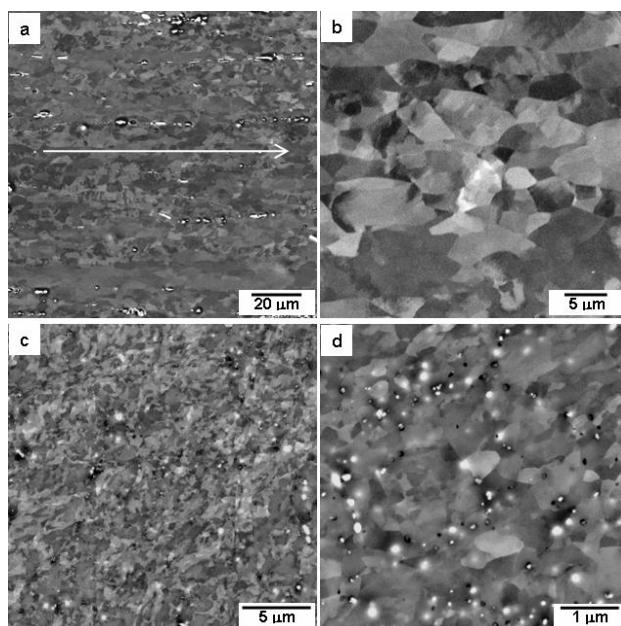
Figure 2. Backscattered electron micrographs of the microstructure of the Al 6101 alloy wire rod: (**a**, **b**) initial state (T1); and (**c**, **d**) after ECAP-C (an arrow indicated the strain direction).

A homogeneous UFG microstructure with a grain size varying from 400 to 600 nm was formed in the wire rods after six ECAP-C cycles at 130 °C (Figures 2c,d and 3a,b). Grains were somewhat elongated along the shear plane. Distribution of spots along the rings on selected area electron diffraction (SAED) patterns shows the formation of grain-type structure with grain boundaries exhibiting mostly high-angle misorientation (Figure 3a) according to [33,34]. In the earlier work [40], the electron backscatter diffraction (EBSD) analysis was applied to study the evolution of grain structure during ECAP processing of an Al-Mg-Si alloy with the similar chemical composition. It was shown that ultra-fine substructure is formed after 1–2 ECAP passes and it is transformed into UFG microstructure with predominant high-angle grain boundaries after four ECAP passes and saturates with further processing.
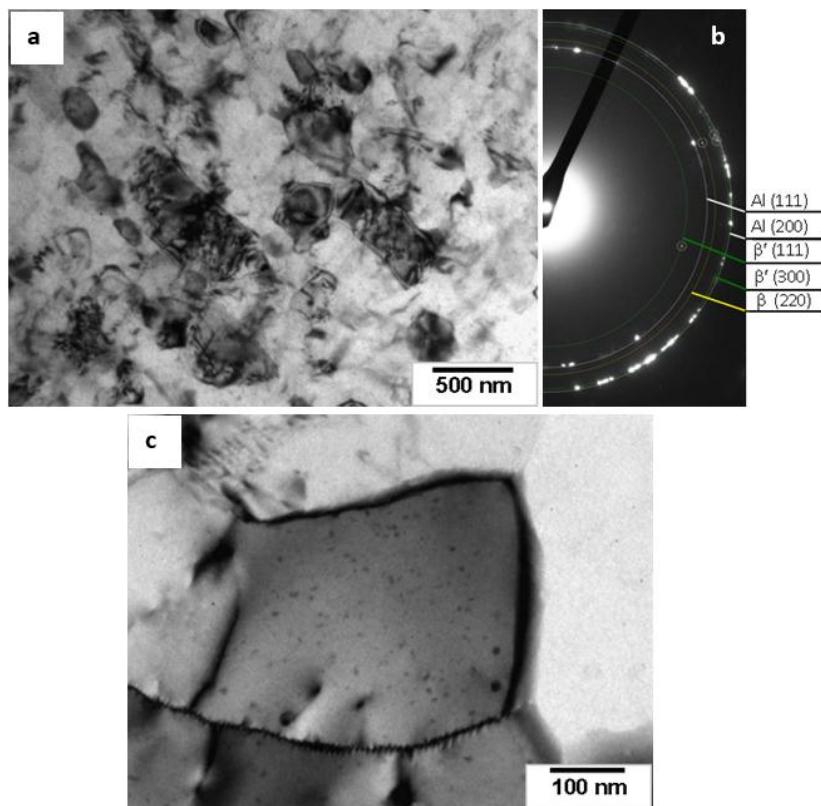
Figure 3. (**a**) Microstructure and (**b**) SAED patterns of the Al 6101 alloy after ECAP-C; and (**c**) view of strengthening second-phase precipitates formed in the matrix of the Al alloy after ECAP-C processing.

TEM studies revealed spherical disperse particles varying from 3 nm to 20 nm in size formed as a result of ECAP-C processing (Figure 3c). Their morphology same as in the previous research [19,22,41,42] on the Al-Mg-Si alloys subjected to SPD under similar temperature conditions indicates that the particles found in the Al 6101 alloy can be regarded as metastable β'-phase precipitates with hexagonal lattice with a Mg/Si ratio of 1.8 [13]. Analysis of SAED patterns (Figure 3b) shows that a part of the spots corresponding to the Al matrix, there are also spots related to the β'-precipitates, as well as β-precipitates with a Mg/Si ratio of 2. Figure 3c represents nanoscale precipitates distributed uniformly within the grain. The size of the precipitates increases considerably

near GBs (Figure 3c). The same pattern of spherical β′-precipitates distribution can be observed in the UFG Al-Mg-Si alloys processed via ECAP-PC or conventional ECAP at 100 °C [22,41,42], whereas β-precipitates were observed in the Al-Mg-Si alloy processed by HPT at 130 °C [23]. These precipitates point to the fact that the UFG structure formation during ECAP-C was accompanied by solid solution decomposition due to the dynamic aging (DA). It has also been previously observed in various Al-Mg-Si alloys during SPD both at elevated [19–24,41–45] and room temperature [23,24,46].

The structure processed via ECAP-C features a high dislocation density (ρ) of about ~8 × 10^{13} m^{-2} according to the X-ray analysis data (Table 1). This accounts for a small size of coherent scattering regions (*D*), as well as for a high mean-square microdistortion of the alloy crystalline lattice ($<\varepsilon^2>^{1/2}$) (Table 1). A considerable reduction in the Al matrix lattice parameter (*a*) after ECAP-C is also observed as compared to rolled wire in state T1 processed via the conventional technique (Table 1).

Table 1. Results of the X-Ray diffraction analysis of the Al 6101 alloy in the initial state (T1), after ECAP-C and ECAP-C + AA.

State	*D* (nm)	$<\varepsilon^2>^{1/2}$ (%)	*a* (Å)	ρ (m^{-2})
Initial state—T1 (this work)	-	-	4.0531 ±0.0008	-
6 cycles ECAP-C at 170 °C	165 ±20	0.110 ±0.024	4.0520 ±0.0002	8.0 × 10^{13}
ECAP-C + AA at 170 °C	188 ±13	0.067 ±0.031	4.0508 ±0.0004	4.3 × 10^{13}

These results are consistent with the phase composition changes observed in the wire rods after ECAP-C by TEM (Figure 3c). This points to a notable decrease in the concentration of Mg and Si in the Al matrix [19,22,42].

ECAP-C processing of a wire rod led to not only the formation of UFG structure and strengthening phase, but also to the distortion of a linear orientation of crystallized intermetallic particles (Figure 2c). A more uniform nature of their distribution was observed, which could reduce to a certain degree the anisotropy of the material mechanical properties [38]. Such a redistribution of intermetallic particles in the Al matrix is possibly the result of SPD [26].

3.2. Mechanical Properties and Electrical Conductivity of the Alloy Processed via ECAP-C

Figure 4 and Table 2 demonstrate the mechanical properties of UFG rolled wire processed via ECAP-C, as well as its properties in T1 state. The Table 2 also contains the values of specific electrical resistivity found experimentally and calculated electrical conductivity values (% IACS). Physical and mechanical properties of Al 6101 alloy in the form of rods and wire produced by different manufacturers are given in Table 2 for comparison. The results gained show that the formation of UFG microstructure in the wire rod enhances the yield strength and the yield stress by ~2.3 and 1.5 times, correspondingly, as compared to the counterparts processed via the conventional technique in state T1 and T4. The formation of UFG structure leads to not only the enhancement of mechanical strength but also to the considerable increase in electrical conductivity. Additionally, UFG wire rods are much stronger than those of the Al 6101 alloy in T6 state (Table 2).

Table 2. Mechanical properties and electrical conductivity of the Al 6101 alloy.

State	YS (MPa)	UTS (MPa)	El$_{total}$ (%)	Resistivity [3] (Ω mm^2/m)	IACS (%)
Initial state—T1 (this work)	120 ±1	195 ±2	22.0 ±0.4	0.03423	50.4
UFG wire rods produced by ECAP-C + AA					
6 passes ECAP-C at 130 ℃	282 ±8	308 ±9	15.1 ±0.6	0.03242	53.1
ECAP-C + AA at 170 ℃	291 ±10	304 ±3	15.0 ±0.3	0.03020	57.1
ECAP-C + AA at 190 ℃	261 ±6	288 ±4	16.8 ±0.9	0.03001	57.4
Wire 3.2 mm in diameter produced from UFG rods					
ECAP-C + AA at 170 ℃ + drawing (diam. 3.2 mm)	-	364 ±9	3.5 ±0.2	0.03055	56.4
Conventionally produced continuous cast redraw rolled rods					
T1 [2]	-	≥190	≥17	≤0.03500	49.3
T4 [1]	-	180–205	15	0.03316	52.0
Wire produced by conventional thermal/thermomechanical treatment					
T6 [1]	-	205–250	-	0.03135	55.0
T81 [1]	-	305–315	6	0.03253	53.0
AL2 (diam. 3.0–5.0 mm) [5]	-	315	3.0	0.03284	52.5
AL7 (diam. 3.0–3.5 mm) [5]	-	275	3.0	0.03050	56.5

T1—Cooled from an elevated temperature shaping process and naturally aged; T4—Solution heat treated and naturally aged; T6—Solution heat treated and artifically aged; T81—Solution heat treated, cold-worked and artificially aged; [1] aluminum continuous cast re-draw rod and wire produced by Southwire (Carrollton, GA, USA) [47]; [2] aluminum continuous cast re-draw rod produced by NPA Skawina (Poland) [48]; [3] electrical resistivity at 20 ℃.
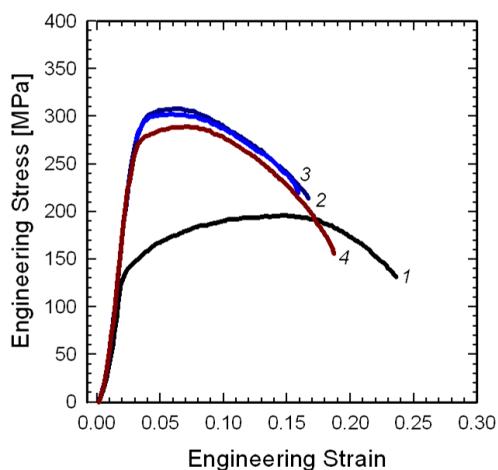

Figure 4. Typical engineering stress—engineering strain curves from tensile testing of the Al 6101 alloy (1) in the T1 condition; (2) after ECAP-C processing; (3) after ECAP-C processing and AA at 170 ℃ for 12 h; and (4) after ECAP-C processing and AA at 190 ℃ for 6 h.

3.3. Properties and Microstructure of the UFG Alloy Processed via Artificial Aging

In [22,23] it was found that a notable enhancement of electrical conductivity in UFG Al-Mg-Si alloys after SPD treatment could be achieved by further artificial aging (AA). There has also been noted that AA can lead to both strength and ductility increases in UFG alloys [22,42,44,49], or only to

mechanical strength enhancement with an admissible ductility decrease [41]. Following these findings a part of the ECAP-C processed wire rod was subjected to AA at 170 ℃ and 190 ℃—the temperatures that are typically used in traditional heat treatment procedures of the commercial rods/wire of 6101 alloy [2,6–8,50].

Figure 5 demonstrates the electrical conductivity dependence on the temperature and the time of AA for UFG wire rods. It can be seen that AA results in a considerable enhancement of electrical conductivity up to over 57% IACS (Figure 5, Table 2). It is obvious that the increase in AA temperature notably reduces the time necessary to achieve high electrical conductivity. The measurements taken revealed that the best possible combination of strength (UTS over 304 MPa), ductility (15.1%), and electrical conductivity (57.1% IACS) are demonstrated by the UFG wire rods processed by AA at 170 ℃ for 12 h. The given level of properties is considerably higher than that of the alloy processed via the conventional techniques (Table 2).
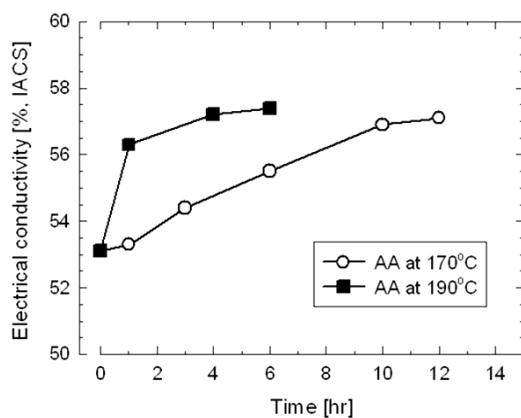
Figure 5. Change in electrical conductivity of test samples of the Al 6101 rod wire after ECAP-C and AA over time.

TEM microstructural studies of the wire rods after ECAP-C and further AA revealed the same grain size as for the SPD-processed material. Metastable β'-second-phase precipitates formed in the grain interior following aging are of a spherical form with a diameter of up to 5 nm and with a length varying from 10 to 50 nm oriented along <001> direction of the Al matrix (Figure 6). A corresponding typical SAED pattern is presented in Figure 6b. Symmetrical streaks between the diffraction spots of [001] Al are related to HCP β'-precipitates [51,52]. Their morphology and location are typical of coarse-grained alloys of the Al-Mg-Si system processed by quenching and further AA [9–13]. Precipitates of the same morphology were observed after AA in UFG Al-Mg-Si alloys processed via ECAP-PC [19,22,42] and HPT [23]. In the research [19,22,42], it was revealed that the grain interior contained not only β'-precipitates, but also needle-shaped metastable β''-phase. The absence of this phase in UFG 6101 alloy in the current study may result from the application of higher temperature range of AA. The change in the UFG alloy phase composition is accompanied by a considerable (almost by two times) decrease in $\langle\varepsilon^2\rangle^{1/2}$ and ρ values (Table 1). Such variations with no notable change in a grain size suggest that recovery processes take place in the UFG structure [26,34]. Additionally, a considerable decrease in the crystalline lattice parameter (*a*) of the Al matrix is noted (Table 1). The parameter comes close to the value for pure Al (4.0495 A). The found variation of

a points to the further decomposition of solid solution accompanied by the growth of precipitations already formed during ECAP-C and the formation of the new ones. The observed decrease in $<\varepsilon^2>^{1/2}$, ρ, and, particularly, in *a*, is the reason for high electrical conductivity of UFG wire rods (Table 2). Such an interrelation between *a* parameter and electrical conductivity has already been established in the studies [19,21–23].
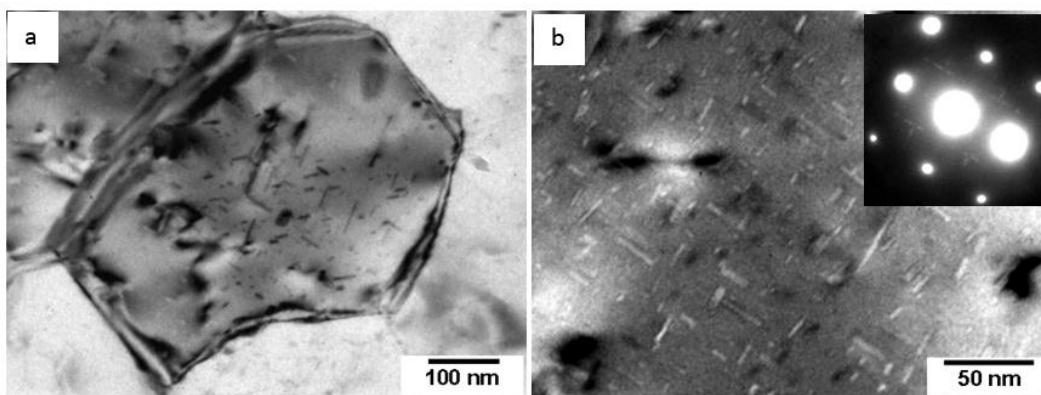
Figure 6. Strengthening second-phase precipitates present in the Al matrix of the ECAP-C processed alloy artificially aged at 170 °C for 12 h: (**a**) bright field TEM image; and (**b**) bright field TEM image and corresponding SAED patterns (the crystal is close to the [001] zone axis orientation).

At present, SPD techniques aimed at processing of commercially applicable UFG metals and alloys with enhanced mechanical and functional characteristics are actively developed [26,53]. The given research demonstrates the possibility to process the specified UFG structure having a unique combination of mechanical strength and electrical conductivity in rods made of Al 6101 alloy using the ECAP-C technique with further artificial aging.

The first processing stage included six cycles (equivalent strain of ~4) of ECAP-C at 130 ℃ by *Bc* route after quenching. The selection of the SPD regime is determined by several reasons.

Firstly, the previous studies showed that SPD processing of Al-Mg-Si alloys under similar conditions led to the formation of a homogeneous UFG structure with enhanced mechanical properties [21,22].

Secondly, it was found that elevated temperature of SPD in Al alloys resulted in a considerable decomposition of solid solution during dynamic aging (DA) accompanied by the formation of nanoscale second-phase precipitates. This led to additional enhancement of both strength and electrical conductivity [21,23].

Thirdly, the selected regimes of SPD provided the capacity for further aging to enhance the properties of UFG alloys. It was shown in the following studies [22,23].

Fourthly, the selected conditions of SPD assure the fabrication of long-length rods with no noticeable macro and/or micro defects.

ECAP-C of wire rods of up to 1.5 m in length resulted in the formation of a homogeneous UFG structure from 400 to 600 nm in size. Additionally, nanoscale spherical metastable β′-second-phase precipitates were formed in the Al matrix during ECAP-C. Their morphological features are typical for

Al alloys, since the formation of ultrafine grains in these alloys is accompanied by the decomposition of solid solution and the formation of strengthening Mg_2Si phases [19–24,41–46]. Their spherical shape is different from the shape of β′-phase (in the form of spheres) formed as a result of a conventional thermal (of T6 type) and/or thermomechanical treatment (of T81 type) of CG counterparts [9–14]. The observed differences are determined by a considerable dislocation activity and the increase in vacancy concentration during SPD (ECAP-C in our case). This leads to a notable increase in the effective diffusion factor in Al alloys [10,54]. The diffusion stepping up accelerates the precipitation kinetics and contributes to the formation of metastable β′-phase after ECAP-C at 130 °C already.

Judging by the character of metastable phase distribution shown in Figure 3b it can be assumed that grain-boundary diffusion plays an important role in the formation and growth of β′-phase metastable precipitates found mainly along GBs. It is well known that the grain-boundary diffusion coefficient is several orders greater than the volume diffusion coefficient [55]. Consequently, the kinetics of the α_{Al}-GB-β″-β′ phase transformation and further enlargement of β′-phase particles formed along GBs is suggested to be controlled by grain-boundary diffusion and is much more enhanced than similar processes inside grains controlled by volume diffusion. Similar character of metastable phase precipitates distribution in UFG Al alloys of the Al-Mg-Si system after SPD treatment was reported in [19,22,23,42].

At the second processing stage of UFG wire rods (after ECAP-C), further AA resulted in the formation of β′-phase precipitates mainly inside grains (Figure 6). This is due to the fact that solute atoms are mostly concentrated inside grains as compared to the regions adjacent to GBs. A similar distribution of metastable phase precipitates was observed in a number of UFG Al-Mg-Si alloys after AA [19,21–23,42]. It is necessary to note that both the current study and the previous research point to the fact that the morphology of metastable phase precipitates in UFG alloys is similar to that of CG counterparts processed by conventional techniques [9–14]. The absence of metastable β″-phase precipitates in the UFG alloy after AA found earlier in Al-Mg-Si alloys after SPD treatment [19,21,22,42] can be explained by the higher aging temperature used to process billets.

The study of the mechanical properties of the UFG alloy shows that the results obtained (Table 2) are in good agreement with microstructural changes taking place after both ECAP-C and further AA. The formation of homogeneous UFG structure (Figures 3 and 6) with mainly large-angle grain boundary misorientations in Al 6101 alloy wire rods after six cycles of ECAP-C at 130 °C resulted in an expected strength enhancement as defined by the Hall-Petch relationship [56,57]. It has been repeatedly confirmed for Al alloys in the UFG state [26,34]. The formation of spherical metastable β′-phase precipitates of ultrafine grains (Figure 4) during AA at 170 and 190 °C does not have any effect on the mechanical properties and even degrades them a little (Table 2). With no noticeable grain enlargement following the aging, this modification of properties in the UFG materials is connected with two competing processes. These are (i) the recovery caused by a considerable decrease in dislocation density (by almost two times) and (ii) the precipitation hardening, due to the formation of metastable β′-phase precipitates inside grains in the course of AA. It was also noted than no strengthening or even certain strength degradation took place in UFG Al-Mg-Si alloys as a result of AA [42]. Spherical β′-phase precipitates formed along GBs of the UFG structure as a result of dynamic aging (DA) play no part in total strengthening of the material [58].

It is well known that electrical conductivity depends on microstructural features of metallic materials determined by electron scattering as a consequence of crystalline structure distortions, including atom thermal vibrations, particles, crystalline lattice defects, *etc.* Thus, it seems very complicated to enhance strength of conductor materials without a significant deterioration of their electrical conductivity using conventional techniques [25]. For example, alloying of pure metals, their strain or precipitation hardening results in a considerable decrease of electrical conductivity due to a notable expansion of electron scattering on grain/sub-grain boundaries, increased amount of solute atoms in the matrix, GP zones, secondary precipitates, and dislocations. It is known that solute atoms in the matrix and GP zones are more efficient in scattering of electrons than other structural elements [25,56]. SPD-processing leads to grain refinement followed by solid solution decomposition and subsequent precipitation and can be used as a new approach to enhance mechanical strength of pure metals with retention of electrical conductivity. It was applied to pure Cu [59,60], and recently has been used to process Cu [61,62] and Al-based alloys [19–23,63]. In our case, DA, in the course of ECAP-C, results in solid solution decomposition, which contributes to certain electrical conductivity enhancement (Table 2). The same effect of DA during SPD was observed in our previous studies [19–23,61]. The dependence of electrical conductivity of UFG Al-Mg-Si alloys on stable Mg_2Si phase precipitates and precipitates of its metastable modifications [19–23] was analyzed. The obtained results suggest that secondary β′ precipitates formed both inside grains and along GBs following ECAP-C have insignificant negative effect on the electrical conductivity of the material under study, while providing significant strengthening effect. Higher amount of Mg atoms are required for formation of β′ precipitates (Mg/Si ratio of 1.8) [13] in comparison with β″ precipitates (Mg/Si ratio of 1.1) [64]. Therefore, β′ precipitates effectively purify the Al matrix from Mg solute atoms, which most negatively affect the electrical conductivity of the material [65]. The formation of new secondary precipitates in the course of AA leads to a further matrix depletion with alloying elements and a more considerable enhancement of UFG 6101 alloy electrical conductivity (Figure 6, Table 2).

Thus, the UFG Al-Mg-Si processed via six ECAP-C cycles at 130 ℃ and AA at 170 or 190 ℃ has electrical conductivity essentially higher than that of counterparts subjected to conventional treatment techniques (Table 2).

It is necessary to note that the unique combination of high mechanical strength and electrical conductivity was achieved in long-length rods through application of ECAP-C. This method appears to be particular promising, especially taking into account first pilot wire samples (Table 2) with an enhanced combination of properties produced from UFG rods by cold drawing modes typically used commercially. Pilot UFG wire samples have UTS of over 360 MPa, elongation to failure of over 3% and electrical conductivity of 56.4% IACS. These studies demonstrate the practical feasibility of a fast transition from pilot rods and wire to their commercial production [66].

4. Conclusions

1. It is demonstrated for the first time that continuous ECAP-C processing can be efficiently used to form the UFG microstructure in Al alloys of the Al-Mg-Si system. ECAP-C with six cycles at 130 ℃ of Al 6101 alloy resulted in the formation of a homogeneous UFG microstructure with a grain size varying from 400 nm to 600 nm in long-length rods.

2. Grain refinement down to ultrafine scale during ECAP-C is accompanied by a dynamic aging leading to the formation of spherical metastable β′-second-phase precipitates and stable β-phase from 3 nm to 20 nm in size.
3. Long-length wire rods made of UFG Al 6101 alloy have much higher mechanical strength as compared to their counterparts processed via conventional treatment techniques. Further artificial aging at 170 ℃ of UFG billets processed via ECAP-C has no effect on their mechanical strength (at 170 ℃) but leads to some strength degradation at 190 ℃.
4. Electrical conductivity of the Al 6101 alloy depends on its microstructural features due to SPD processing. Decomposition of supersaturated solid solution leading to the formation of metastable β′-phase and stable β-phase in the course of ECAP-C as a result of dynamic aging and additional β′-phase during artificial aging is an efficient approach to enhance the electrical conductivity of the alloy. UFG long-length rods were used to produce the wire samples by cold drawing with superior properties considerably exceeding the existing counterparts processed via conventional techniques.

Acknowledgments

Author Contributions

Maxim Murashkin formulated the idea of this work, supervised the workflow and created the initial draft. Andrei Medvedev carried out mechanical tensile tests, conductivity measurements and performed microstructural characterization of the processed material by SEM. Vil Kazykhanov performed microstructural characterization studies of the processed material by TEM, Nariman Enikeev performed microstructural characterization with the help of the X-ray diffraction analysis. Alexandr Krokhin supplied the initial material for study, Georgi Raab processed the wire rods by ECAP-C. Ruslan Z. Valiev contributed with the overall supervision and development of the main concepts presented in this paper. All authors discussed the experimental results, participated in manuscript preparation and approved the final manuscript.

Conflicts of Interest

The authors declare no conflict of interest.

References

1. Nicoud, J.C.; Gaschingard, P. Important recent developments in the manufacture of redraw rod in Almelec (AA-6101 Al-Mg-Si Alloy) for the conductors employed on overhead power transmission and distribution lines. In Proceedings of the Wire Assoc, Asia 82, Singapore, 4–8 October 1982; 43–46.

2. Davies, G. Aluminium alloy (6201, 6101A) conductors. In Proceedings of the International Conference on Overhead Line Design and Construction: Theory and Practice (up to 150 kV), London, UK, 28–30 November 1988; pp. 93–97.

3. Kiessling, F.; Nefzger, P.; Nolasco, J.F.; Kaintzyk, U. *Overhead Power Lines: Planning, Desing, Construction*; Springer-Verlag: Berlin, Germany, 2003.

4. Totten, G.E., MacKenzie, D.S., Eds. *Handbook of Aluminium*; Marcel Dekker: New York, NY, USA, 2003.

5. European Committee for Standardization (CEN). EN 50183, Overhead Power Line Conductors—Bare Conductors of Aluminium Alloy with Magnesium and Silicon Content; CEN: Bruxelles, Belgium, 2002.

6. Koch, S. Aluminum alloys for wire harnesses in automotive engineering. *BHM* **2007**, *152*, 62–67.

7. Cervantes, E.; Guerrero, M.; Ramos, J.A.; Montes, S.A. Influence of natural aging and cold deformation on the mechanical and electrical properties of 6201-T81 aluminum alloy wires. *Mater. Res. Soc. Symp. Proc.* **2010**, *1275*, 75–80.

8. Karabay, S. Modification of AA-6201 alloy for manufacturing conductivity and extra high conductivity wires with property of high tensile stress after artificial aging heat treatment of high for all aluminium alloy conductors. *Mater. Design* **2006**, *27*, 821–832.

9. Edwards, G.A.; Stiller, K.; Dunlop, G.L.; Couper, M.J. The precipitation sequence in Al-Mg-Si alloys. *Acta Mater.* **1998**, *46*, 3893–3904.

10. Murayama, M.; Hono, K.; Saga, M.; Kikuchi, M. Atom probe studies on the early stages of precipitation in Al-Mg-Si alloys. *Mater. Sci. Eng. A* **1998**, *250*, 127–132.

11. Murayama, M; Hono, K. Pre-precipitate clusters and precipitation processes in Al-Mg-Si alloys. *Acta Mater.* **1999**, *47*, 1537–1548.

12. Andersen, S.J.; Marioara, C.D.; Froseth, A.; Vissers, R.; Zandbergen, H.W. Crystal structure of the orthorhombic $U2-Al_4Mg_4Si_4$ precipitate in the Al-Mg-Si alloy system and its relation to the β' and β″ phases. *Mater. Sci. Eng. A* **2005**, *390*, 127–138.

13. Vissers, R.; van Huis, M.A.; Jansen, J.; Zandbergen, H.W.; Marioara, C.D.; Andersen, S.J. The Crystal Structure of the β′ Phase in Al-Mg-Si Alloys. *Acta Mater.* **2007**, *55*, 3815–3823.

14. Pogatscher, S.; Antrekowitsch, H.; Leitner, H.; Ebner, T.; Uggowitzer, P.J. Mechanisms controlling the artificial aging of Al-Mg-Si Alloys. *Acta Mater.* **2011**, *59*, 3352–3363.

15. Wuhua, Y.; Zhenyu, L. Effect of Zr addition on properties of Al-Mg-Si aluminum alloy used for all aluminum alloy conductor. *Mater. Design* **2011**, *32*, 4195–4200.

16. Gupta, A.K.; Lloyd, D.J.; Court, S.A. Precipitation hardening processes in an Al-0.4% Mg-1.3% Si-0.25% Fe aluminum alloy. *Mater. Sci. Eng. A* **2001**, *301*, 140–146.

17. Gupta, A.K.; Lloyd, D.J.; Court, S.A. Precipitation hardening in Al-Mg-Si alloys with and without excess Si. *Mater. Sci. Eng. A* **2001**, *316*, 11–17.

18. Liu, C.H.; Chen, J.; Lai, Y.X.; Zhu, D.H.; Gu, Y.; Chen, J.H. Enhancing electrical conductivity and strength in Al alloys by modification of conventional thermo-mechanical process. *Mater. Design* **2015**, doi:10.1016/j.matdes.2015.07.133.

19. Bobruk, E.V.; Murashkin, M.Y.; Kazykhanov, V.U.; Valiev, R.Z. Aging behavior and properties of ultrafine-grained aluminum alloys of Al-Mg-Si system. *Rev. Adv. Mater. Sci.* **2012**, *31*, 101–115.

20. Sabirov, I.; Murashkin, M.; Valiev, R.Z. Nanostructured aluminium alloys produced by severe plastic deformation: New horizons in development. *Mater. Sci. Eng. A* **2013**, *560*, 1–24.

21. Valiev, R.Z.; Murashkin, M.Y.; Sabirov, I. A nanostructural design to produce high-strength Al alloys with enhanced electrical conductivity. *Scr. Mater.* **2014**, *76*, 13–16.

22. Murashkin, M.; Sabirov, I.; Kazykhanov, V.; Bobruk, E.; Dubravina, A.; Valiev, R.Z. Enhanced mechanical properties and electrical conductivity in ultra-fine grained Al alloy processed via ECAP-PC. *J. Mater. Sci.* **2013**, *48*, 4501–4509.

23. Sauvage, X.; Bobruk, E.V.; Murashkin, M.Y.; Nasedkina, Y.; Enikeev, N.A.; Valiev, R.Z. Optimization of electrical conductivity and strength combination by structure design at the nanoscale in Al-Mg-Si alloys. *Acta Mater.* **2015**, *98*, 355–366.

24. Sha, G.; Tugcu, K.; Liao, X.Z.; Trimby, P.W.; Murashkin, M.Y.; Valiev, R.Z.; Ringer, S.P. Strength, grain refinement and solute nanostructures of an Al-Mg-Si alloy (AA6060) processed by high-pressure torsion. *Acta Mater.* **2014**, *63*, 169–179.

25. Rositter, P.L. *The Electrical Resistivity of Metals and Alloys*; Cambridge University Press: Cambridge, UK, 2003.

26. Valiev, R.Z.; Zhilyaev, A.P.; Langdon, T.G. *Bulk Nanostructured Materials: Fundamentals and Applications*; John Wiley & Sons, Inc.: Hoboken, NJ, USA, 2014.

27. Semenova, I.P.; Polyakov, A.V.; Raab, G.I.; Lowe, T.C.; Valiev, R.Z. Enhanced fatigue properties of ultrafine-grained Ti rods processed by ECAP-Conform November. *J. Mater. Sci.* **2012**, *47*, 7777–7781.

28. Gunderov, D.V.; Polyakov, A.V.; Semenova, I.P.; Raab, G.I.; Churakova, A.A.; Gimaltdinova, E.I.; Sabirov, I.; Segurado, J.; Sitdikov, V.D.; Alexandrov, I.V.; *et al.* Evolution of microstructure, macrotexture and mechanical properties of commercially pure Ti during ECAP-conform processing and drawing. *Mater. Sci. Eng. A* **2013**, *562*, 128–136.

29. Raab, G.J.; Valiev, R.Z.; Lowe, T.C.; Zhu, T.Y. Continuous processing of ultrafine grained Al by ECAP-Conform. *Mater. Sci. Eng. A* **2004**, *382*, 30–34.

30. Xu, C.; Schroeder, S.; Berbon, P.B.; Langdon, T.G. Principles of ECAP-Conform as a continuous process for achieving grain refinement: Application to an aluminum alloy. *Acta Mater.* **2010**, *58*, 1379–1386.

31. Niendorf, T.; Böhner, A.; Höppel, H.W.; Göken, M.; Valiev, R.Z.; Maier, H.J. Comparison of the monotonic and cyclic mechanical properties of ultrafine-grained low carbon steels processed by continuous and conventional equal channel angular pressing. *Mater. Design* **2013**, *47*, 138–142.

32. Segal, V.M. Materials processing by simple shear. *Mater. Sci. Eng. A* **1995**, *147*, 157–164.

33. Langdon, T.G.; Furukawa, M.; Nemoto, M; Horita, Z. Using equal-channel angular pressing for refining grain size. *JOM* **2000**, *52*, 30–33.

34. Valiev, R.Z.; Langdon, T.G. Principles of equal-channel angular pressing as a processing tool for grain refinement. *Prog. Mater. Sci.* **2006**, *51*, 881–981.

35. Lutterotti, M.; Matthies, S.; Wenk, H.R. MAUD (Material Analysis Using Diffraction): A user friendly Java program for Rietveld Texture Analysis and more. In Proceeding of the 12th International Conference on Textures of Materials (ICOTOM-12), Montreal, QC, Canada, 9–13 August 1999; p. 1599.

36. Williamson, L.K.; Smallman, R.E. III. Dislocation densities in some annealed and cold-worked metals from measurements on the X-ray Debye--Scherrer spectrum. *Phil. Mag.* **1956**, *1*, 34–45.

37. International Electrotechnical Commission (IEC). *IEC 60468: Method of Measurement of Resistivity of Metallic Materials*; IEC: Geneva, Switzerland, 1974.

38. Mondolfo, L.F. *Aluminum Alloys: Structure and Properties*; Butterworths: London, UK, 1976.

39. Hatch, J.E. *Aluminum: Properties and Physical Metallurgy*; ASM International: Metals Park, OH, USA, 1984.

40. Mackenzie, P.W.J.; Lapovok, R. ECAP with back pressure for optimum strength and ductility in aluminium alloy 6016. Part 1: Microstructure. *Acta Mater*. **2010**, *58*, 3198–3211.

41. Sauvage, X.; Murashkin, M.Y.; Valiev, R.Z. Atomic scale investigation of dynamic precipitation and grain boundary segregation in a 6061 aluminium alloy nanostructured by ECAP. *Kov. Mater. Met. Mater.* **2011**, *49*, 11–15.

42. Bobruk, E.V.; Kazykhanov, V.U.; Murashkin, M.Y.; Valiev, R.Z. Enhanced strengthening in ultrafine-grained Al-Mg-Si alloys produced via ECAP with parallel channels. *AEM* **2015**, doi:10.1002/adem.201500119.

43. Roven, H.J.; Liu, M.; Werenskiold, J.C. Dynamic precipitation during severe plastic deformation of an Al-Mg-Si aluminium alloy. *Mater. Sci. Eng. A* **2008**, *483–484*, 54–58.

44. Kim, W.J.; Kim, J.K.; Park, T.Y.; Hong, S.I.; Kim, D.I.; Kim, Y.S.; Lee, J.D. Enhancement of strength and superplasticity in a 6061 Al alloy processed by equal-channel-angular-pressing. *Metall. Mater. Trans. A* **2002**, *33*, 3155–3164.

45. Kashyap, B.P.; Hodgson, P.D.; Estrin, Y; Timokhina, I.; Barnett, M.R.; Sabirov, I. Plastic flow properties and microstructural evolution in an ultrafine-grained Al-Mg-Si alloy at elevated temperatures. *Metall. Mater. Trans. A* **2009**, *40*, 3294–3303.

46. Nurislamova, G.; Sauvage, X.; Murashkin, M.; Islamgaliev, R.; Valiev, R. Nanostructure and related mechanical properties of an Al-Mg-Si alloy processed by severe plastic deformation. *Philos. Mag. Lett.* **2008**, *88*, 459–466.

47. Southwire®. Available online: http://www.southwire.com (accessed on 25 May 2015).

48. NPA Skowina. Available online: http://www.npa.pl (accessed on 13 April 2015).

49. Roven, H.J.; Nesboe, H.; Werenskiold, J.C.; Seibert, T. Mechanical properties of aluminium alloys processed by SPD: Comparison of different alloy systems and possible product areas. *Mater. Sci. Eng. A* **2005**, *410–411*, 426–429.

50. Aluminum Association. *Aluminum Standarts and Date*, 2nd ed.; Aluminum Association: Washington, DC, USA, 1986.

51. Dutta, I.; Allen, S.M. A calorimetric study of precipitation in commercial aluminium alloy 6061. *J. Mater. Sci. Lett.* **1991**, *10*, 323–326.

52. Cai, M.; Field, D.P.; Lorimer, G.W. A systematic comparison of static and dynamic ageing of two Al-Mg-Si alloys. *Mater. Sci. Eng. A* **2004**, *373*, 65–71.

53. Fakhretdinova, E.; Raab, G.; Ryzhikov, O.; Valiev, R. Processing ultrafine-grained aluminum alloy using Multi-ECAP-Conform technique. *IOP Conf. Ser. Mater. Sci. Eng.* **2014**, doi:10.1088/1757-899X/63/1/012037.

54. Genevois, C.; Fabregue, D.; Deschamps, A.; Poole, W.J. On the coupling between precipitation and plastic deformation in relation with friction stir welding of AA2024 T3 aluminium alloy. *Mater. Sci. Eng. A* **2006**, *441*, 39–48.

55. Frost, H.J.; Ashby, M.F. Deformation-Mechanism Maps: The Plasticity and Creep of Metals and Ceramics; Pergamon Press: Oxford, UK, 1982.

56. Hall, E.O. The deformation and ageing of mild steel: III Discussion of results. *Proc. Phys. Soc.* **1951**, *64*, 747–752.

57. Petch, N.J. The cleavage strength of polycrystals. *J. Iron Steel Inst.* **1953**, *174*, 25–28.

58. De, P.S.; Su, J.Q.; Mishra, R.S. A stress-strain model for a two-phase ultrafine-grained aluminum alloy. *Scr. Mater.* **2011**, *64*, 57–60.

59. Takata, N.; Lee, S.H.; Tsuji, N. Ultrafine grained copper alloy sheets having both high strength and high electric conductivity. *Mater. Lett*. **2009**, *63*, 1757–1760.

60. Zhang, Y.; Li, Y.S.; Tao, N.R.; Lu, K. High strength and high electrical conductivity in bulk nano-grained Cu embedded with nano-scale twins. *App. Phys. Lett.* **2007**, doi:10.1063/1.2816126.

61. Islamgaliev, R.K.; Nesterov, K.M.; Bourgon, J.; Champion, Y.; Valiev, R.Z. Nanostructured Cu-Cr alloy with high strength and electrical conductivity. *J. Appl. Phys.* **2014**, doi:10.1063/1.4874655.

62. Valiev, R.Z.; Sabirov, I.; Zhilyaev, A.P.; Langdon, T.G. Bulk nanostructured metals for innovative applications. *JOM* **2012**, *64*, 1134–1142.

63. Murashkin, M.Y.; Sabirov, I.; Sauvage, X.; Valiev, R.Z. Nanostructured Al and Cu alloys with superior strength and electrical conductivity. *J. Mater. Sci.* **2015**, doi:10.1007/s10853-015-9354-9.

64. Hasting, H.S.; Frøseth, A.G.; Andersen, S.J.; Vissers, R.; Walmsley, J.C.; Marioara, C.D.; Danoix, F.; Lefebvre, W.; Holmestad, R. Composition of β″ precipitates in Al-Mg-Si alloys by atom probe tomography and first principles calculations. *J. Appl. Phys.* **2009**, doi:10.1063/1.3269714.

65. Kutner, F. *Aluminium—Monograph, Aluminium Conductor Materials*; Aluminium-Verlag GmbH: Duesseldorf, Germany, 1981; pp. 15–27.

66. Mann, V.K.; Krokhin, A.Y.; Matveeva, I.A.; Raab, G.I.; Murashkin, M.Y.; Valiev, R.Z. Nanostructured wire rod research and development. *Light Met. Age* **2014**, *72*, 26–29.